Torque Control of Electrorheological Fluidic Actuators for Haptic Vehicular Instrument Controls

Marie-Aude Vitrani, Jason Nikitczuk, Guillaume Morel, Constantinos Mavroidis

Proceedings of the 2004 IEEE
International Conference on Robotics & Automation
New Orleans, LA • April 2004

Torque Control of Electrorheological Fluidic Actuators for Haptic Vehicular Instrument Controls

Vitrani M. A.[A], Nikitczuk J.[B], Morel G.[A], Mavroidis C.[B,1]

[A] Laboratoire de Robotique de Paris (LRP)
18, route du Panorama - BP 61
92265 Fontenay-aux-Roses Cedex
Tel. : (+33) 01 46 54 78 12; Fax : (+33) 01 46 54 72 99
Email: morel@robot.jussieu.fr,
Webpage: http://www.robot.jussieu.fr/

[B] Department of Mechanical and Industrial Engineering
375 Snell Engineering Center, Northeastern University
360 Huntington Avenue, Boston MA 02115
Tel: 617-373-4121, Fax: 617-373-2921
Email: mavro@coe.neu.edu
Webpage: http://www.coe.neu.edu/~mavro

[1] Author for Correspondence

Abstract– **Force-feedback mechanisms have been designed to simplify and enhance the human-vehicle interface. The increase in secondary controls within vehicle cockpits has created a desire for a simpler, more efficient human-vehicle interface. By consolidating various controls into a single, haptic feedback control device, information can be transmitted to the operator, without requiring the driver's visual attention. In this paper, the experimental closed loop torque control of Electro-Rheological Fluids (ERF) based actuators for haptic application is performed. ERFs are liquids that respond mechanically to electric fields by changing their properties, such as viscosity and shear stress, electroactively. Using the electrically controlled rheological properties of ERFs, we developed actuators for haptic devices that can resist human operator forces in a controlled and tunable fashion. In this study, the ERF actuator analytical model is derived and experimentally verified and accurate closed loop torque control is experimentally achieved using a non-linear proportional integral controller with a feed-forward loop.**

Index Terms– Torque Control; Electro-Rheological Fluids; Advanced Actuators; Haptic Systems.

I. Introduction

In recent years, the proliferation of secondary controls within vehicles has created a desire to develop mechanisms to simplify and enhance the human-vehicle interface. A better interface technology is sought to facilitate driver access to a growing array of vehicle secondary functions, such as advanced audio features, climate controls, telecommunications and navigation. Electro-Rheological Fluids (ERF) based force-feedback mechanisms have been developed to address these issues. ERFs are liquids that respond mechanically to electrical stimulation by changing their viscosity electroactively. Using the electrically controlled rheological properties of ERFs, haptic devices have been developed that can resist human operator forces in a controlled and tunable fashion.

Instrument controls have haptic properties to maximize the ease of use for vehicle occupants. A single force-feedback knob can emulate the feel of conventional control knobs (detents, limit stops, friction) and can produce new effects as well such as vibration, scrolling, and free-spin, all instantaneously reconfigurable under computer control. Such a haptic knob can simulate the functions of all instrument controls that it replaces and thus reduced to one device, the control of the dashboard provides the driver with instant access to all functions, quickly and ergonomically.

Several rotary force-feedback control knobs have been proposed for use in vehicular control that use a motor and a microprocessor controller to achieve the desired effect [1-4]. However, the magnitude of the torque available from these devices is limited by the size of the motor and its power consumption, both of which must be limited for practical use in a vehicle. To address some of these issues, a haptic knob has been developed that incorporates a brake to provide high torque capability in a small volume with low power consumption [5]. A Magneto-Rheological fluid (MRF)-based brake actuator [6] improves the performance characteristics, however a large magnetic circuit is needed to generate a sufficient actuating magnetic field. By using Electro-Rheological Fluids it is possible to overcome the remaining limitations to further enhance the development of haptic interfaces for vehicular control. Specifically, it is possible to decrease the size, weight and power consumption while increasing torque / force capability and device degrees-of-freedom. Of special importance is the latter characteristic that will increase the "dexterity" of the force-feedback device by being able to program a larger number of functions.

Electro-Rheological Fluid (ERF) exhibit a rapid, reversible and tunable transition from a fluid state to a solid-like state upon the application of an external electric field [7]. Some of the advantages of ERFs are their high yield stress, low current density, and fast response (less than 1 millisecond). ERFs can apply very high electrically controlled resistive forces while their size (weight and geometric parameters) can be very small. ERFs can be combined with other actuator types such as electromagnetic, pneumatic or electrochemical actuators so that novel, hybrid actuators are produced with high power density and low energy requirements [8].

Kenaley and Cutkosky proposed the use of ERFs for tactile sensing in robotic fingers [9]. Based on that work, several workers proposed the use of ERFs in tactile arrays used to interact with virtual environments [10] and also as assistive devices for the blind to read the Braille system as proposed by Monkman [11]. Continuing this work, Professor Taylor and his group at the University of Hull, UK, developed and tested experimentally a 5x5 ERF tactile array [12]. Professor Furusho and his group at Osaka University in Japan, proposed an ERF-based planar force-feedback manipulator system that

interacts with a virtual environment [13]. This system is actuated by low-inertia motors equipped with an ER clutch. An ERF-based force-feedback joystick has been developed in Fraunhofer-Institut in Germany. The joystick consists of a ball and socket joint where ERF has been placed in the space between the ball and the socket. The operator feels a resistive force to his/her motion resulting in from the controlled viscosity of the ERF [14].

While a lot of work has been performed on the design, modeling and testing of ERF based actuators and devices; very little work has been performed on the closed loop control of these devices. All of the existing work in this area concerns the position control [15] while no work has been performed on the force / torque control of these devices. ERF devices are generally used with position control as dampers to avoid vibration [16], as example in vehicle suspension [17] or for anti-seismic building [18]. Position control has also been used in ERF based valves [19].

Our group has developed and studied several ERF based actuators and haptic systems [20, 21]. Recently we developed prototypes of rotary ERF based actuating elements for haptic knobs for vehicular instrument controls [22]. In the present study, the ERF actuator analytical model is derived and experimentally verified and accurate closed loop torque control is experimentally achieved using a non-linear proportional integral controller with a feed-forward loop. In addition, we demonstrate the ability of such an apparatus to exhibit realistic haptic illusions, such as a programmable range of the knob, or position programmable "clicks".

II. FUNDAMENTALS OF ERF MODELLING

ERFs are suspensions of polarizable particles in viscous non-conducting oil with particle-fluid dielectric mismatch [23]. Since the discovery of the electrorheological phenomenon, a lot of research has been performed to develop a behaviour model of ERF. The well known one is the Bingham model.

Under zero field conditions ERFs are generally characterized by a simple Newtonian viscosity [24]. When subjected to high electric fields, ERFs develop a yield stress and their shear stress τ is fairly well modelled as a Bingham plastic:

$$\tau = \mu\dot{\gamma} + \tau_{y,d} \quad (1)$$

where μ is the plastic viscosity, $\dot{\gamma}$ is the shear rate and $\tau_{y,d}$ is the Bingham or dynamic yield stress.

One can conclude by extrapolation to zero shear rate that the stress must exceed this dynamic yield stress in order for the material to flow, similarly to a dry coulomb friction model. In fact, the minimum stress required to cause the ERF to flow is not necessarily the dynamic yield stress but rather the static yield stress $\tau_{y,s} > \tau_{y,d}$. Using the friction analogy, this can be understood as the well-known Stribeck effect. More precisely, there are three yield stresses characterizing the behaviour of an ERF [25]. The first is the elastic-limit yield stress τ_e, which is used, in solid mechanics. Upon complete removal of stress exceeding τ_e, the material never fully recovers and suffers a permanent strain γ_e, which is the transition between elastic and plastic deformation. The elastic-limit yield stress is not the limit of linear behaviour but rather the limit of reversibility for the material. Loss of linear behaviour generally occurs before the elastic limit. The static yield stress τ_s is the minimum stress necessary for the unbounded strain or the deformation of the material. Finally the plateau stress for large strains is the dynamic yield stress τ_d.

When a shear thinning or thickening effect is more pronounced, the post-yield behaviour becomes non linear. In order to accurately model this non linear post-yield (or flowing) behaviour, another generic fluid model should be used that is called the Herschel-Bulkley model [26]:

$$\tau = \tau_{y,d} + k\dot{\gamma}^n \quad (2)$$

This fluid model is a generalized model for visco-plastic flow with yield stress. It can be reduced to the Bingham plastic model (namely, n=1) in the case where post-yield shear thinning or thickening are minimal.

In regard to the Bingham model described by Equation 1, the applied electric field E affects the dynamic yield stress, with a quadratic relationship. This yields:

$$\tau_{y,d} = \alpha E^2 \quad (3)$$

The ERF used in this project is the LID 3354S manufactured by Smart Technology Ltd. [27]. It is made up of 35% by volume of polymer particles in silicone/fluorolube base oil. According to the provider, the field dependencies for this particular fluid are:

$$\begin{cases} \tau_{y,s} = C_s (E - E_{ref}) \\ \tau_{y,d} = C_d E^2 \\ \mu = \mu_0 - C_v E^2 \end{cases} \quad (4)$$

Where μ_0 is the zero field viscosity, C_s, C_d, C_v and E_{ref} are constants which approximate values are supplied by the manufacturer. Obviously, the formula for the static yield stress is only valid for fields greater than E_{ref}. In this work, it is assumed that the torque controller will be used to finely control the resistive torque of a device that is moved by an operator (or by an auxiliary motor) and therefore only the dynamic mode is considered.

III. ERF ACTUATOR AND EXPERIMENTAL SYSTEM

A haptic feedback joystick and knob has been developed by our team to address the desire for simplifying and enhancing the human-vehicle interface [22]. These devices rely on passive, revolute ERF-based actuators to induce controllable resistive torques. These actuators are used in this paper as the test-bed to perform closed loop torque control experiments and initial haptic knob tests.

The studied ERF actuator consists of multiple parallel rotating electrode plates to enhance the resistive torque output capability of the actuator by increasing the activated area of the fluid while maintaining a compact volume. Figure 1 shows a cut-away view and a picture of the assembled multiple Flat-Plate or FP actuator. Applying an electric field across the gaps causes the fluid properties to change, resulting in an increase in yield stress. This property is used to control the force feedback of the actuator. The plastic parts of the prototype were built using rapid prototyping methods to allow for the quick creation of complicated shapes that would not have been possible with machine shop methods. Table 1 shows the important parameters of the FP actuator prototype.

To test the performance of the FP actuator prototype, to experimentally validate its theoretical model and to perform

closed loop torque control experiments the actuator was incorporated into an experimental setup, shown in Figure 2. The actuator shaft is attached to a flexible coupling to ensure proper alignment. The other side of the flexible coupling is connected to a DC motor through a belt with a pulley wheel. This motor applies known external torques to the FP actuator that will controllably resist these externally applied torques. An optical encoder attached to the shaft is used to measure the angular displacement. A torque sensor is attached at the base of the FP actuator to measure its resistive torque output. In this experimental setup, two parameters can be changed by the user: the motor velocity and the voltage applied to the fluid.

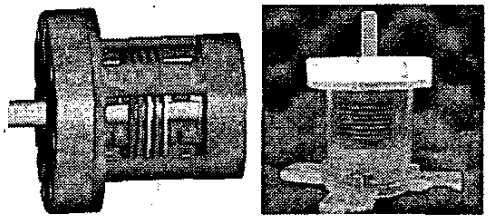

Fig. 1 Assembled Multiple Flat-Plate ERF Actuator: CAD Drawing (Left) & Prototype (Right)

TABLE 1: SUMMARY OF ERF ACTUATOR PROPERTIES

	FP actuator
Outer radius	14.7 mm
Length	32.5 mm
Gap width	.5 mm
Dynamic Torque at 2 kV	188.5 mN m
Dynamic Torque at 4 kV	753.4 mN m
Range of motion	120°
Number of Plates	15

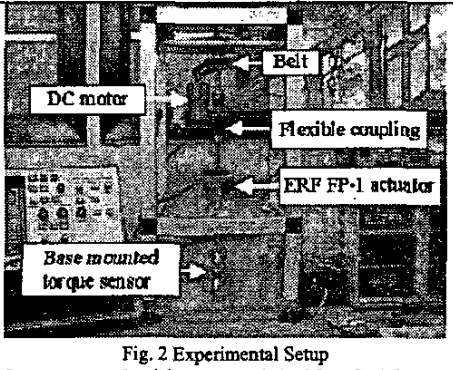

Fig. 2 Experimental Setup

A PC augmented with a US Digital® PC7166™ PC to incremental encoder interface card and a Datel® PC-412C™ Analog I/O board was used in the open and closed loop experiments. The PC collects the sensor measurements, through the data acquisition board or the encoder interface card, performs the feedback control calculation and then it sends out the signal to the FP actuator, through the D/A converter and laboratory built amplifiers. WinRec v.1, software developed in our laboratory, provides deterministic fast timers based on MSDN library under Windows NT platforms and can be used in both real-time control and data acquisition.

IV. FP ACTUATOR MODEL

Modelling of ERF actuators for use in closed loop torque control is inexistent. Therefore our first step was to develop a model of the ERF actuator used that is suitable for closed loop torque control. Figure 3 defines important geometric parameters that are used in the model. Since the system is mostly to be used when flowing, the post-yield model (i.e. dynamic mode) is derived. Providing an actuator model from the fluid model supposes to map the shear stress into the output torque and the shear rate into the output velocity. To do so, we assume that the shear stress is constant along a line parallel to the axis, between the electrodes. Also, due to the symmetry of the system, the shear stress is supposed to depend only on the radius r, not on the angle θ.

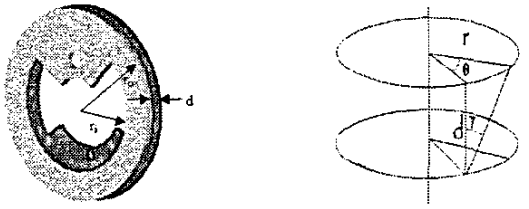

Fig. 3 FP Actuator Model Important Parameters

The elementary resistive torque between a pair of electrodes is then:

$$T_{ele} \approx \int_{r_i}^{r_o} r\tau(r)dA \qquad (5)$$

where $dA = 2\pi r dr$ and $\tau(r)$ is the shear stress at a radius r from the axis.

Since N rotating plates are mounted in between of N+1 fixed plates, there are 2N gaps filled with ERF, producing a total resistive torque given by:

$$T = 2NT_{ele} \approx 4\pi N \int_{r_i}^{r_o} r^2\tau(r)dr \qquad (6)$$

Furthermore, for a displacement $\delta\theta$ of the actuator, the (angular) shear deformation of a fluid element $\delta\gamma$ (see Figure 3) at a radius r is:

$$\delta\gamma = \frac{r}{d}\delta\theta \qquad (7)$$

The relationship from the actuator angular velocity to the shear rate is then:

$$\dot{\gamma} = \frac{r}{d}\dot{\theta} \qquad (8)$$

Thus, combining Equations (1), (4), and (8), one gets:

$$\tau(r) = C_d E^2 + (\mu_0 - C_v E^2)\frac{r}{d}\dot{\theta} \qquad (9)$$

Combining with Equation (6), one gets:

$$T = 4\pi N \int_{r_i}^{r_o} r^2 (C_d E^2 + (\mu_0 - C_v E^2)\frac{r}{d}\dot{\theta})dr \qquad (10)$$

which finally leads to:

$$T = 4\pi N\left[C_d \frac{r_o^3 - r_i^3}{3} - C_v \frac{r_o^4 - r_i^4}{4d}\dot{\theta}\right]E^2 + \pi N(r_o^4 - r_i^4)\frac{\mu_0}{d}\dot{\theta} \qquad (11)$$

Furthermore, in order to produce the electric field, a positive voltage is applied to the fixed plates, while the rotating plates, which geometrically alternate with the fixed ones, are grounded. The field is then the same in all the inter-plate gaps, and is simply given by:

$$E = \frac{V}{d} \tag{12}$$

The final model can then be written as:

$$T = (\alpha_0 - \alpha_1\dot{\theta})V^2 + \alpha_2\dot{\theta} \tag{13}$$

where α_i, $i \in [1,...3]$ are constant positive scalars given by:

$$\begin{cases} \alpha_1 = \dfrac{\pi 4 N C_d (r_0^3 - r_i^3)}{3d^2} \\ \alpha_1 = \dfrac{\pi N C_v (r_0^4 - r_i^4)}{d^3} \\ \alpha_2 = \pi N (r_0^4 - r_i^4)\dfrac{\mu_0}{d} \end{cases} \tag{14}$$

V. Experimental Parameter Identification

Our objective here is to verify the ability of Equation (13) to describe the post-yield behaviour of the actuator and experimentally identify the model parameters. First experiments are done with a constant speed of the DC motor that provides the input torque to the FP actuator. Then the same experiments are performed with different constant speeds. In order to avoid the excitation of internal hysteretic cycles, that would corrupt the parametric identification; a careful repetitive procedure is used as follows for each experiment with constant speed: a) the actuator is initially placed at $\theta = 0°$; b) the motor starts and obtains a constant velocity, and a ramp voltage is applied to the ERF. It is verified that the ramp slope is slow enough compared to the expected actuator dominant dynamics. As a result, a quasi-static behaviour can be assumed. When applying the ramp voltage, the resistive torque is measured; c) when this experiment is over, the actuator is put back in the initial position with a null electric field; d) it is then verified that, redoing the experiment from step a, the torque response is repeatable.

On Figure 4, lines in blue show typical results of the torque-voltage relationship for two different velocities of the DC motor. From Figure 4 it can be verified that the response shape agrees with Equation (13). It can be noticed that, below a certain voltage limit V_{lim} which depends on the velocity, the ERF seems reactionless. Note that this is in accordance with Equation (4), which describes the static pre-yield behaviour, although what is measured here is the dynamic mode. To account for this experimentally emphasized phenomenon, and taking into account that the experiments were performed with constant speed, then Equation (13) could be written as:

$$T = \begin{cases} T_0 & \text{if} \quad V < V_{lim} \\ T_0 + k\ (V - V_{lim})^2 & \text{otherwise} \end{cases} \tag{15}$$

where T_0 is the minimal torque measured with a zero voltage, V_{lim} is the voltage under which nothing happens.

The three parameters of a constant speed experiment, namely T_0, k, and V_{lim} are then computed in order to obtain a least square best fit. In Figure 4, the red lines show the best fits of this model for the different velocities. The identified parameters T_0, k, and V_{lim} are different for each experiment, which denotes their dependency on velocity. In turn, a best fit is used to express the velocity dependency of these three parameters. It is found that the three parameters are linear functions of the velocity. Namely:

$$T = T_0 + k(V - V_{lim})^2 \text{ with } \begin{cases} T_0 = 17.25\text{sign}(\dot{\theta}) + 0.0625\dot{\theta} \\ k = 123\text{sign}(\dot{\theta}) + 0.5\dot{\theta} \\ V_{lim} = \begin{cases} 0.3 + 7.10^{-4}\dot{\theta} & \text{if } \dot{\theta} < 0 \\ 0.45 - 7.10^{-4}\dot{\theta} & \text{if } \dot{\theta} > 0 \end{cases} \end{cases} \tag{16}$$

where V is the computer output voltage expressed in Volts (which is also the ERF applied voltage expressed in kV) and the torques are expressed in mNm. Note that the velocity dependency confirms, in part, the theoretical model. For example, the coefficient k decreases with the velocity, as the expected effect of the positive scalar α_1. Some discrepancies can also be noticed. For example, the zero field torque T_0 is not reduced to a pure viscosity, as expected. Rather, there is a dry friction term (17.25 mNm).

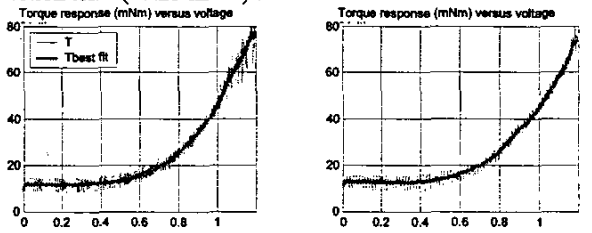

Fig. 4 Reactive Torque Response vs. Velocity

The open and closed loop controllers will be using the actuator model identified with Equation (16) to convert desired torques to input voltages in the actuator. To do so Equation (16) needs to be "inversed" so that it calculates the voltage V as a function of the command torque $\tilde{T}$ and of the actuator velocity $\dot{\theta}$:

$$V(\tilde{T},\dot{\theta}) = V_{lim}(\dot{\theta}) + \sqrt{\frac{\tilde{T} - T_0(\dot{\theta})}{k(\dot{\theta})}} \tag{17}$$

To be able to use Equation (17) the following constraint needs to be satisfied:

$$T(V,\dot{\theta}) - T_0(\dot{\theta}) \geq 0 \tag{18}$$

Inequality (18) means that the desired resistive torque that the actuator should produce must be larger than $T_0(\dot{\theta})$, i.e. the minimal torque measured with a zero voltage, which is the sum of a dry friction term and a viscous term depending on the velocity. In cases where the desired torque is such that Inequality (18) is not satisfied, i.e. when the applied voltages are between zero and V_{lim}, a linear interpolation is used to calculate the applied voltage:

$$V(\tilde{T},\dot{\theta}) = V_{lim}(\dot{\theta})\frac{\tilde{T}}{T_0(\dot{\theta})} \tag{19}$$

Equation (19) does not correspond to any physical model, but it is used in the open and closed loop control to provide model continuity when the voltages are lower than the voltage V_{lim} where the ERF is reactionless.

VI. Closed Loop Control

A non-linear, model based, PI controller with a feedforward term was implemented as shown in Figure 5. A control error is fed into a PI controller. The command torque is the sum of the output from the PI controller and a desired

torque feedforward term. The latter is used so that the PI compensator works with small values of inputs and outputs. The command torque is converted to a control voltage using the non-linear Equation (17). Some representative results from the experiments with this controller are shown in Figure 6. It can be clearly seen that the response is fast (settling time is approx. 70 ms) and well damped. A residual error remains due to a dead zone of 0.07mNm that was put in order to avoid the excitation of hysteretic cycles. The response is reproducible for any value of the desired torque input which indicates a successful linearization. Extensive experiments have demonstrated a strong robustness of the controller to variations of experimental conditions, such as the magnitude and sign of velocity. The closed loop dynamics are rather constant, even when the actuator is cycled arbitrarily, i.e. when its hysteretic behaviour is excited.

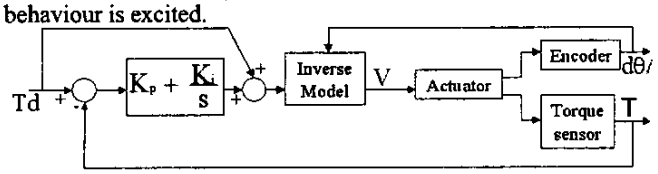

Fig. 5 Non Linear PI Controller With Feed-Forward Term

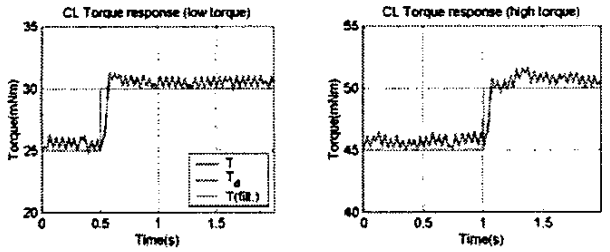

Fig. 6: Closed loop Step Response Using a Non-Linear PI Controller

VII. Creating A Haptic Sensation

A major difficulty in creating a haptic sensation with ERF-based actuators is that they are semi-active systems i.e. they act as a controllable brake with variable and controllable damping and can not produce an effective torque or generate a displacement. ERF-based actuators can only change their viscosity in order to resist externally applied forces or torques by a user. Thus, achieving a haptic sensation with an ERF based actuator, it is required to implement a haptic function that uses as inputs not only the knob angle, but also the measurement of the torque applied by the operator.

We consider here the haptic realization of a "click" function. Namely, what we want to provide is a minimal resistive torque over the knob angular range, except around a given position θ_0 where it has to click. Consider that the operator moves the knob with a positive velocity. Up to a certain angle $\theta_1 < \theta_0$, the desired torque is zero. Then, when $\theta_1 < \theta < \theta_0$, the system should resist increasingly, while, if $\theta > \theta_0$, the desired torque should instantaneously drop to zero in order to produce the feeling of a rapid release. Thus, for a positive motion:

$$\begin{cases} \text{if } \theta_1 < \theta < \theta_0 \\ \quad \text{then if } T > 0 \\ \qquad \text{then } T_d = T_{max}\dfrac{\theta - \theta_1}{\theta_0 - \theta_1} \\ \qquad \text{else } T_d = 0 \\ \text{else } T_d = 0 \end{cases}$$

Note that, even if $\theta_1 < \theta < \theta_0$ the desired torque is set to zero when the applied torque is negative, which allows to pull back the knob with no resistance if the user does not want to push over the click. In order to feel the click for both directions of rotation at the same position, it is required to implement a symmetric function for positions larger than θ_0 and negative torques, as illustrated in Figure 7. Furthermore, in order to prevent the torque loop integrator from saturating when the operator releases the knob within the angular click domain, the torque controller output V is frozen whenever the applied torque is zero. Such a zero torque is actually detected within a dead zone of ± 1.5 mNm, so as to deal with the measurement noise. Finally, the following algorithm is used to compute the desired torque:

$$\begin{cases} \text{if } \theta_1 < \theta < \theta_0 \\ \quad \text{then if } T > 1.5 \\ \qquad \text{then } T_d = T_{max}\dfrac{\theta - \theta_1}{\theta_0 - \theta_1} \\ \qquad \text{else if } T < -1.5 \\ \qquad\quad \text{then } T_d = 0 \\ \qquad\quad \text{else } V_{k+1} = V_k \\ \text{else if } \theta_0 > \theta > \theta_2 \\ \quad \text{then if } T < -1.5 \\ \qquad \text{then } T_d = T_{max}\dfrac{\theta_2 - \theta}{\theta_2 - \theta_0} \\ \qquad \text{else if } T < -1.5 \\ \qquad\quad \text{then } T_d = 0 \\ \qquad\quad \text{else } V_{k+1} = V_k \\ \text{else } T_d = 0 \end{cases} \tag{20}$$

The parameters θ_0, θ_1, θ_2 and T_{max}, can be tuned to produce different feelings. T_{max} represents the maximum resistance. Reducing the width $\theta_2 - \theta_1$ would produce a quicker click sensation. However, this parameter has to be tuned considering also the dynamics of the torque loop and the maximum velocity of the knob. Indeed, if the operator rapidly turns the knob and the programmed width is small, there is a risk that the reaction of the torque loop, which starts when $\theta > \theta_1$, is not completed when $\theta > \theta_0$. In this case, the desired torque comes back to zero and the click is not felt by the operator.In addition to the inner non-linear PI torque controller, Algorithm (20) has been implemented, with the following parameters: $\theta_0 = 60$ deg, $\theta_1 = 55$ deg, $\theta_2 = 65$ deg and $T_{max} = 60$ mNm. To produce illustrative plots of the system behaviour, experiments were performed using the DC motor as an operator, thus producing a well controllable velocity.

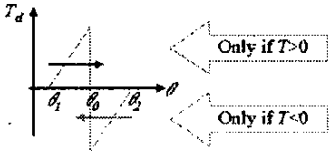

Fig. 7 The Haptic Function of a "Click"

In a representative haptic experiment shown in Figure 8, the click is passed one time in both directions. It can be observed that the desired torque is a ramp since the velocity is constant. The actual torque precisely follows the desired one, except when the desired torque is zero, which cannot be achieved by the actuator due to the minimal amount of friction. This minimal amount, which is different before and after the click, is due to the hysteretic effect. The click-release dynamics are very fast, as the actual torque drops to its minimal amount within less than 100ms.

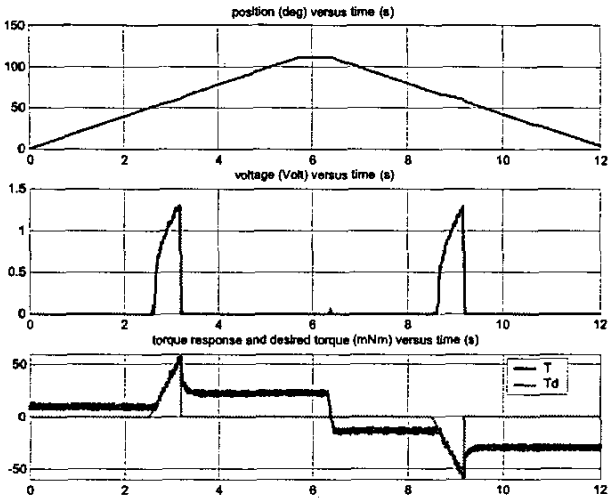

Fig. 8 Haptic Sensation: Passing Through a "Click"

VIII. CONCLUSIONS

The purpose of this research was to verify the possibility of using ERF based actuators in haptic interfaces. An experimental method has been proposed to identify the system model that describes the resistive torque as a function of both the applied voltage and the velocity. The experimental inverse model was added to a PI controller in order to linearize the system. It has been shown that this non-linear PI controller with feed-forward exhibits a precise and accurate response, making it well-suited for haptic applications. Then, a function using the measured position, velocity and torque has been derived to attain the sensation of a knob with detents, or clicks. This function has been combined with the previous controller to create a unique haptic interface. Experiments following emphasized the high quality haptic sensations possible from combining these actuators with the discussed controllers and functions.

ACKNOWLEDGEMENTS

This work was supported by the National Science Foundation (DMI-9984051, CMS-0301338, CMS-0422720). Any opinions, findings, conclusions or recommendations expressed in this publication are those of the authors and do not necessarily reflect the views of the National Science Foundation.

REFERENCES

1. BMW iDrive Controller: http://www.bmwworld.com/models/e65.htm , 2002
2. Kuenzner, H. et al., "Operating Device for Menu Controlled Functions of a Vehicle", US005,956,016, September 1999.
3. Levin, M. et al., "Control Knob with Multiple Degrees of Freedom and Force Feedback", US006,154,201, Nov. 2000.
4. Mannesmann VDO AG Information Systems, "Programmable Rotating Actuator with Haptic Feedback", www.vdo.com .
5. Badescu M., Wampler C., and Mavroidis, C., " Rotary Haptic Knob for Vehicular Instrument Controls", *Proc. of the 10th Symp. on Haptic Interfaces for Virtual Environment and Teleoperator Systems,* March 24 & 25, 2002, Orlando Florida.
6. Ackermann B. and Elferich, R., "Application of Magnetorheological Fluids in Programmable Haptic Knobs", *Actuator 2000, 7th International Conference on New Actuators,* June 19-21, 2002 – Bremen, Germany.
7. Phule P. and Ginder J., "The Materials Science of Field-Responsive Fluids," *MRS Bulletin*, Aug. 1998, pp. 19-21.
8. Mavroidis C., Bar-Cohen Y. and Bouzit M., "Chapter 19: Haptic Interfaces Using Electrorheological Fluids", Invited Chapter in *Electroactive Polymer (EAP) Actuators as Artificial Muscles: Reality, Potentials and Challenges*, Y. Bar-Cohen Editor, SPIE Optical Engineering Press, February 2001, pp. 567-594.
9. Kenaley G. L. and Cutkosky M. R., "Electrorheological Fluid-Based Robotic Fingers With Tactile Sensing," *Proceedings of the 1989 IEEE International Conference on Robotics and Automation,* Scottsdale AR, pp. 132-136.
10. Wood D., "Tactile Displays: Present and Future," *Displays-Technology & Applications*, Vol. 18, No. 3, 1998, pp. 125-128.
11. Monkman G. J., "Electrorheological Tactile Display", *Presence*, MIT Press, Vol. 1, No. 2, 1992.
12. Taylor P. M., Hosseini-Sianaki A. and Varley C. J., "Surface Feedback for Virtual Environment Systems Using Electrorheological Fluids," *International Journal of Modern Physics B,* Vol. 10, No. 23 & 24, 1996, pp. 3011-3018.
13. Sakaguchi M. and Furusho J., " Force Display System Using Particle-Type Electrorheological Fluids," *Proceedings of the 1998 IEEE International Conference on Robotics and Automation,* Leuven, Belgium, May 1998, pp. 2586-2590.
14. Böse H., Berkemeier J. and Trendler A., "Haptic System Based on Electrorheological Fluid," *Proceedings of the ACTUATOR 2000 Conference,* 19-21 June 2000, Bremen GERMANY.
15. Choi SB., "Control of ER devices", *International Journal of modern physics B* vol 13 Nos 14,15 and 16, (1999) 2160-2167
16. Powell JA., "ERF as a Means of Vibration Suppression", *Proc. of Int. Conf. on Vibration and Noise,* April 25-27, 1995, pp 1-8.
17. Rettig U. and Von Stryk O., "Numerical Optimal Control Strategies for Semi-Active Vehicle Suspension with ERF Dampers" In: K.-H. Hoffmann, R.H.W. Hoppe, V. Schulz (eds.): Fast Solution of Discretized Optimization Problems (Birkhauser Verlag 2001) pp. 221-241.
18. Gavin HP., "Control of Seismically-Excited Vibration Using ER Materials and Lypunov Methods" *IEEE Transactions and Automatics Control*, Vol. 9, No. 1, pp. 27-36, 2001.
19. Nakano M., Minagawa S., and Hagino K., "PMW Flow Rate Control of ER Valve and its Application to ER Actuator Control" *International Journal of Modern Physics B* Vol 13 Nos 14-16, (1999), pp. 2168-2175.
20. Fisch A., Mavroidis C., Melli-Huber J. and Bar-Cohen Y., "Chapter 4: Haptic Devices for Virtual Reality, Telepresence, and Human-Assistive Robotics", Invited Chapter in *Biologically-Inspired Intelligent Robots*, Eds.: Y. Bar-Cohen and C. Breazeal, SPIE Press, pp. 73-101, 2003.
21. Mavroidis C., Pfeiffer C., Celestino J. and Bar-Cohen Y., "Design and Modeling of an Electro-Rheological Fluid Based Haptic Interface," *Proc. of the 2000 ASME Mechanisms and Robotics Conference,* Baltimore, MD, September 10-13, 2000.
22. Melli-Huber J., Weinberg B., Fisch A., Nikitczuk J., Mavroidis C., Wampler C., " Electro-Rheological Fluidic Actuators for Haptic Vehicular Instrument Controls", *Proc. of the 11th Symp. on Haptic Interf. for Virtual Environment and Teleoperator Sys.*, March 22 and 23, 2003, Los Angeles, CA, pp. 262-267.
23. Block, H. and Kelly, J. P., "Electro-Rheology", *Journal of Physics, D: Applied Physics,* Vol. 21, 1988, pp. 1661.
24. Rajagopal KR., Ruzicka M., "Mathematical Modelling of ER Materials", *Continuum Mech. Thermodyn.* 13: pp. 59-78.
25. Bonnecaze and Brady, "Yield Stresses in Electrorheological Fluids", *Journal of Rheology,* 36,73-115, 1992.
26. Wang and Gordaninejad, "Flow Analysis of Field-Controllable, Electrorheological and Magnetorheological Fluids Using Herschel-Bulkley Model", *J. of Intelligent Materials, Systems and Structures,* Vol.10, pp. 601-608, 1999.
27. Smart Technology Ltd, "Technical Information Sheet – Electro-Rheological Fluid LID 3354S", 2001.